Mathematical Modeling and Algorithm Application
ISSN: 3006-0842 | Vol. 7, No. 3, 2025

CGPR: A Study on a Spatiotemporal Temperature Prediction Model for Henan Based on Improved PredRNN with ChebConv

Zhongcai Li*

School of Computer Science and Technology, Henan Polytechnic University, Jiaozuo, China.

* **Corresponding author**: Zhongcai Li (Email: 212309010009@home.hpu.edu.cn)

Abstract: As a major agricultural province, accurate temperature prediction in Henan is of great importance. This paper proposes a new model called ChebConv PredRNN (CGPR), which combines a graph neural network with a spatiotemporal recurrent neural network. First, the original gridded meteorological data is modeled as a graph structure to capture complex spatial correlations. Second, the PredRNN architecture is improved by replacing the traditional spatial convolutional layers with Chebyshev graph convolution (ChebConv). Experiments based on historical data from 2015 to 2018 demonstrate that the model significantly outperforms baseline models such as LSTM, ConvLSTM, and the original PredRNN in prediction accuracy, proving the effectiveness of graph structure modeling in spatiotemporal temperature sequence prediction.

Keywords: Temperature prediction; PredRNN; Chebyshev graph convolution; ConvLSTM.

1. Introduction

Temperature prediction (TP) is one of the core tasks in weather forecasting and is of great significance for agricultural production, energy scheduling, disaster warning, and more. Located in central China, Henan experiences a transitional climate from warm temperate to subtropical, with an average annual temperature of 12.8–15.5°C, an average July temperature of 27–28°C, and an average January temperature of –2 to 2°C, exhibiting distinct spatiotemporal heterogeneity. However, achieving accurate TP is challenging. On the temporal scale, temperature variations are influenced by multiple physical elements such as solar radiation and wind speed. Although these changes exhibit certain regularities, they are also accompanied by non-stationarity and random fluctuations, making stable prediction difficult. On the spatial scale, temperature changes do not occur in isolation. The temperature at a given location is affected by neighboring regions and even distant areas, and this complex spatial correlation further complicates the prediction task. To date, various methods have been proposed for temperature prediction. Existing approaches can be broadly categorized into two groups: time series models and spatiotemporal data models. Time series models learn patterns of temperature variation from data to construct prediction models, assuming that the internal dynamics and external driving factors of temperature are embedded in their long-term sequential data. By identifying hidden patterns in historical observations, these models are used for future data prediction. Statistical models, such as linear regression models[1][2], and commonly used machine learning methods, such as Markov models[3][4], genetic algorithms[5][6][7], and support vector machines[8][9][10], are included in this category. However, these methods have limited capability in extracting complex nonlinear relationships, leading to relatively low prediction accuracy. Deep learning, on the other hand, can automatically extract useful features from large volumes of data without manual intervention and possesses strong nonlinear fitting capabilities, making it widely used in temperature prediction. Examples include Long Short-Term Memory networks(LSTM)[11][12][13], MLP[14][15], and Transformer models[16]. As an improved version of recurrent neural networks, LSTM controls the input, forgetting, and output of data at different time steps through gating mechanisms, demonstrating excellent capability in processing sequential data. Its variants, such as BiLSTM[17] and sLSTM[18], have shown strong performance in different sequential tasks. However, the models mentioned above process only one-dimensional time series data and do not consider spatial features, leaving room for improvement in prediction accuracy. Spatiotemporal information fusion-based prediction methods break through performance bottlenecks by integrating spatiotemporal correlations, i.e., comprehensively considering the influence of overall spatial effects on target observation points. Models such as ConvLSTM[19], TGCN[20], 3D-CNN[21], MAU[22], and PredRNN[23] have shown excellent performance in spatiotemporal temperature prediction. However, due to limitations of traditional convolution operations in handling grid data—such as fixed receptive fields and difficulty in modeling long-range dependencies—the ability to extract spatiotemporal correlations remains constrained, and prediction accuracy still requires improvement. In summary, time series models exhibit poor prediction performance due to their neglect of spatiotemporal features, while existing spatiotemporal models have limitations in extracting spatiotemporal features, resulting in insufficient prediction accuracy. To address this issue, this paper proposes a novel spatiotemporal prediction model called ChebConv PredRNN (CGPR) for temperature prediction in Henan. The contributions of this paper are as follows:

1.Using spatiotemporal data for temperature prediction and constructing the grid-based temperature data into a spatiotemporal graph structure, where nodes represent grid points and edges represent spatial adjacency relationships.

2.Adopting the ST-LSTM unit and zigzag memory flow mechanism of PredRNN to capture temporal dynamics.

3.Replacing traditional convolution with ChebConv graph convolution (K=5) to better model spatial dependencies.

The structure of the paper is as follows: Section 2 introduces the fundamental principles of the model. Section 3 describes the dataset and experimental parameter settings. Section 4 presents, discusses, and analyzes the experimental results of the proposed prediction method. Section 5 summarizes the main conclusions.

2. Methodology

2.1. Graph Representation of Spatiotemporal Data

The original grid points are regarded as the nodes V of the graph to construct an undirected graph G = (V, E), where the node features are the daily temperature observations. An adjacency matrix A is also constructed, and the edge relationships are defined using the 8-neighborhood algorithm, meaning each grid point is connected to its surrounding 8 points. This representation allows the model to break through the rectangular constraints of traditional convolution kernels. E is the set of edges between the nodes, with edge weights set to 1. Its Laplacian matrix is defined as L = D - A, where A is the adjacency matrix and D is the degree matrix.

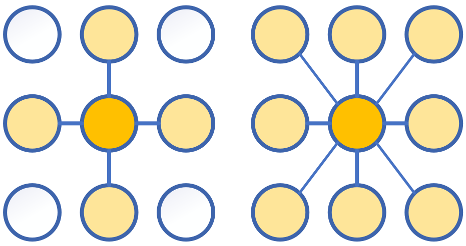

Figure 1: Four-neighborhood and eight-neighborhood.

2.2. ChebConv

In the spectral domain, graph convolution can be expressed as the product of the signal X and the filter g_θ. ChebConv approximates the filter using a K-order Chebyshev polynomial, and the output Z of the convolutional layer is calculated as:

$$Z=\sum_{k=0}^{K-1}\Theta_k\, T_k(\hat{L})X \tag{1}$$

Where: $X \in R^{n\times d}$ is the input temperature feature matrix, with n representing the number of grid cells and d denoting the number of features. Here, as only temperature features are considered, d = 1. Θ_k is the learnable weight parameter for the k-th order polynomial. K is the order of the convolution kernel, representing the receptive field of the spatial convolution (i.e., considering neighbors up to the (K-1)-th order around the central site). $\hat{L}$ is the rescaled Laplacian matrix, intended to map the eigenvalues to the interval [-1, 1] to ensure numerical stability. It is defined as follows:

$$\hat{L}=\frac{2}{\lambda_{max}}L-I_n \tag{2}$$

where λmax is the maximum eigenvalue of L, and In is the identity matrix. The Chebyshev polynomials $T_k(\hat{L})$ can be efficiently computed using the following recurrence formula:

$$T_k(\hat{L})=2\hat{L}T_{k-1}(\hat{L})-T_{k-2}(\hat{L}) \tag{3}$$

In this paper, traditional convolution employs fixed-size convolution kernels (e.g., 3×3, 5×5), which can only capture local neighborhood information, resulting in limited receptive fields. For the temperature grid regions in Henan, spatial dependencies between different grid points may span multiple grids, making it difficult for fixed receptive fields to model long-range spatial correlations. In contrast, ChebConv approximates spectral convolution using Chebyshev polynomials. Setting K=5 means that it can capture information from up to the 5th-order neighborhood, effectively modeling longer-range spatial dependencies. This multi-scale spatial information aggregation capability enables the model to better understand the complex topography and climatic characteristics of Henan (such as the temperature differences between the mountainous areas of western Henan and the Nanyang Basin).

2.3. CGPR Model

The core innovation of PredRNN lies in the introduction of the Spatiotemporal Memory Flow mechanism, a zigzag-style memory propagation approach that allows memory states to propagate vertically between stacked RNN layers while also propagating horizontally along the temporal dimension. This addresses the issue in traditional ConvLSTM models where memory states are confined within each layer, preventing effective communication between layers. The fundamental building block of PredRNN is the ST-LSTM unit, which incorporates a dual-memory mechanism on the basis of the traditional LSTM. Temporal Memory: Flows horizontally within the same layer, capturing long-term temporal dependencies. Spatiotemporal Memory: Flows vertically between layers, capturing short-term spatiotemporal dynamics. Building on this, to address the limitations of standard convolution, the 2D convolution is replaced with ChebConv, resulting in a novel CGST-LSTM unit. Its formulas are as follows:

$$\begin{aligned}
&g_t=\tanh(W_{xg}**X_t+W_{hg}**H_{t-1}^{l}+b_g)\\
&i_t=\sigma(W_{xi}**X_t+W_{hi}**H_{t-1}^{l}+b_i)\\
&f_t=\sigma(W_{xf}**X_t+W_{hf}**H_{t-1}^{l}+b_f)\\
&C_t^l=f_t\odot C_{t-1}^{l}+i_t\odot g_t\\
&g_t'=\tanh(W_{xg}'**X_t+W_{mg}**M_t^{l-1}+b_g')\\
&i_t'=\sigma(W_{xi}'**X_t+W_{mi}**M_t^{l-1}+b_i')\\
&f_t'=\sigma(W_{xf}'**X_t+W_{mf}**M_t^{l-1}+b_f')\\
&M_t^l=f_t'\odot M_t^{l-1}+i_t'\odot g_t'\\
&o_t=\sigma(W_{xo}**X_t+W_{ho}**H_{t-1}^{l}+W_{co}**C_t^l+W_{mo}**M_t^l+b_o)\\
&H_t^l=o_t\odot\tanh(W_{1\times1}**[C_t^l,M_t^l])
\end{aligned} \tag{4}$$

where ** denotes ChebConv graph convolution, ⊙ denotes the Hadamard product, X_t denotes the input tensor at time step t, H_{t-1}^{l} denotes the hidden state of the l-th layer at time t-1, C_t^l denotes the temporal memory cell (horizontal transmission) of the l-th layer, M_t^l denotes the spatial memory cell (vertical transmission) of the l-th layer, σ denotes the Sigmoid activation function, and W_{**} denotes the learnable convolution weight parameters. The model is illustrated in Figure 2:

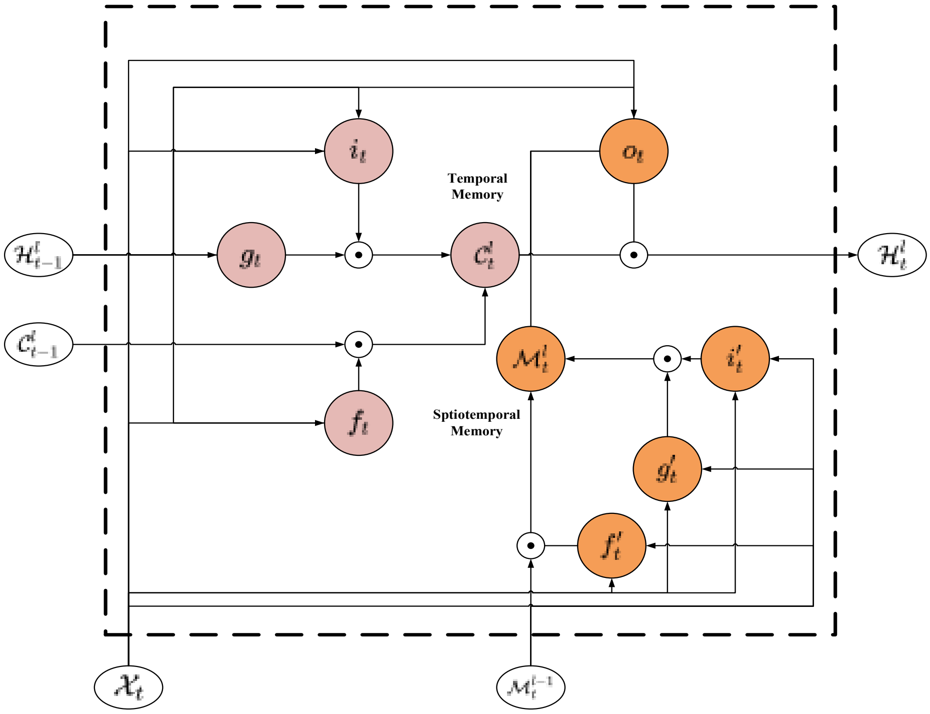

Figure 2: CGST-LSTM module.

The CGPR model constructed from the CGST-LSTM module is illustrated in Figure 3. Specifically, the model is built using a 4-layer CGST-LSTM module, which produces different outputs at distinct time steps.

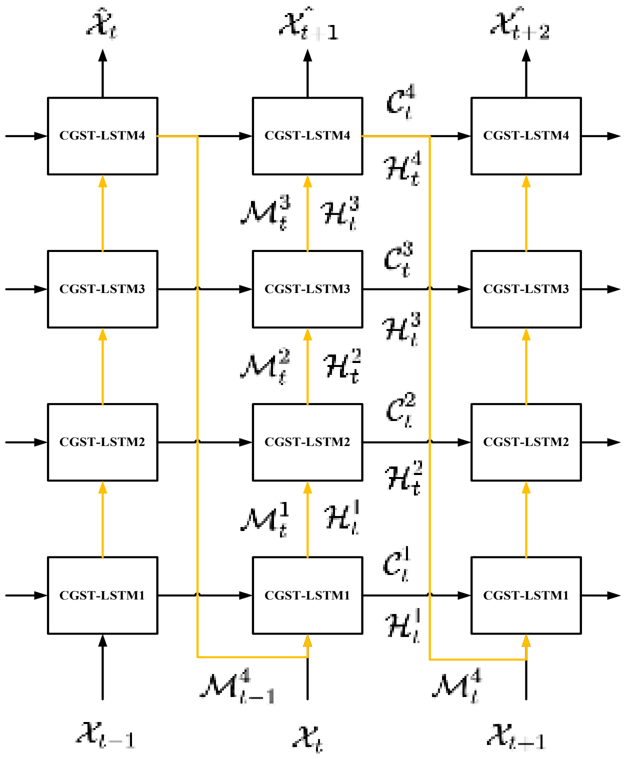

Figure 3: CGPR model.

3. Experimental Setup

3.1. Study Area

In temperature prediction, the study area is typically divided into equally sized grid cells based on longitude and latitude. The temperature records for each grid cell are obtained from observation devices within that cell. All grid cells form an R*C matrix, representing the temperature at a specific time point Ti, where R and C correspond to the number of grid cells along the longitude and latitude directions, respectively. This matrix is then converted into a graph structure, resulting in X_i. All matrices derived from historical temperature records form a time series X_1, X_2, ..., X_t.

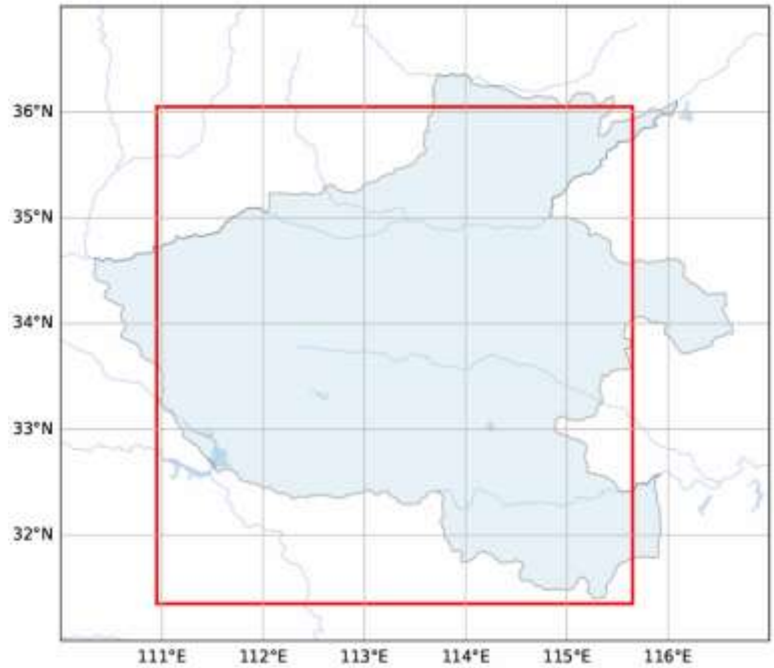

Figure 4: Henan Study Area

Figure 4 shows the Henan study area. The temperature data for Henan is sourced from the China Regional Surface Meteorological Elements Driving Dataset provided by the National Tibetan Plateau Scientific Data Center, covering the period from 2015 to 2018. After data selection and segmentation, the raw matrix data for Henan is obtained, with the study area spanning [31.35°N–36.15°N, 110.95°E–115.75°E]. The area is divided into 48*48 grids, with a spatial resolution of 0.1°*0.1° and a temporal resolution of 3 hours. The total number of samples is 11,688. The raw data is then converted into a graph structure based on this framework.

3.2. Model Parameter Settings and Model Evaluation Metrics

In this paper, LSTM, ConvLSTM, PredRNN, TGCN, and MAU are used as comparative models. Among them, LSTM, ConvLSTM, PredRNN, and CGPR are RNN-based architectures. To eliminate the influence of parameters, the number of layers for LSTM, ConvLSTM, PredRNN, and CGPR is uniformly set to 4.

The input window size for all models is 8. For the Henan dataset, given the hourly temporal resolution and the complexity of spatiotemporal changes influenced by numerous factors, an excessively long output window would lead to substantial errors, rendering the results less meaningful. Therefore, the output window size is set to 1. During training, the Adam optimizer is employed, with the learning rate set to 0.0001, and an early stopping mechanism is implemented with a patience value of 10. All experiments are conducted on a high-performance server equipped with a 14-core Xeon(R) Gold 6330 CPU and 2 NVIDIA GeForce RTX 3090 GPUs, utilizing Python and PyTorch.

To comprehensively evaluate the prediction results of the models, we use Mean Squared Error (MSE) and Mean Absolute Error (MAE) as the evaluation metrics. The formulas are as follows:

$$MSE=\frac{1}{n}\sum_{i=1}^{n}(y_i-\hat{y}_i)^2 \tag{5}$$

$$MAE=\frac{1}{n}\sum_{i=1}^{n}|y_i-\hat{y}_i| \tag{6}$$

Mean Squared Error (MSE) measures the average magnitude of the squared differences between predicted and observed values, with a range from zero to positive infinity. In the model evaluation framework, a smaller MSE value indicates superior predictive performance, as it reflects a reduction in residual variance. Mean Absolute Error (MAE) quantifies the arithmetic mean of the absolute prediction deviations, employing a linear scoring rule that assigns equal weight to each error. It provides a direct measure of the average size of prediction errors without considering their direction. Better model performance is reflected in smaller values, as this indicates a reduction in the average magnitude of prediction errors. All these metrics adhere to the principle of error minimization, where lower values (closer to zero) signify higher model fidelity and better consistency with the true measured values.

4. Experimental Analysis

4.1. The Spatiotemporal Prediction Superiority of CGPR

Table 1 demonstrates the prediction capabilities of different models for one-step temperature forecasting on the Henan dataset. CGPR comprehensively outperforms all baseline models in both MSE (Mean Squared Error) and MAE (Mean Absolute Error). Compared to the classic ConvLSTM, CGPR reduces MSE by approximately 11.9%. Compared to the currently strongest spatiotemporal baseline model, PredRNN, CGPR lowers the MSE from 1.606 to 1.561, and the MAE drops below the 0.9 threshold. This validates that the improvement of replacing 2D convolution with Chebyshev graph convolution is highly effective.

Table 1: Model Prediction Results

Model	MSE	MAE
LSTM	2.248	1.095
ConvLSTM	1.773	0.986
MAU	2.224	1.111
TGCN	2.317	1.113
PredRNN	1.606	0.922
CGPR	**1.561**	**0.897**

PredRNN employs fixed-weight 2D convolution kernels, which are unable to adaptively adjust spatial weights when processing the 48 * 48 grid of Henan's diverse terrain (western mountains, eastern plains). CGPR, with ChebConv (K=5), captures nonlinear spatial dependencies across a wider geographical range, thereby achieving greater precision in capturing details of temperature fluctuations. Observations show that the pure graph-based model TGCN (2.317) performs even worse than ConvLSTM (1.773). Although TGCN uses a graph structure, its temporal processing capability is relatively weak. Temperature prediction requires robust long- and short-term memory flow. Experiments demonstrate that simply having a "graph" is insufficient; the powerful spatial feature extraction capability of graph convolution must be integrated with PredRNN's spatiotemporal memory flow architecture (i.e., the proposed CGPR) to achieve optimal results. A comparison with MAU and LSTM reveals that LSTM lacks spatial dimension modeling, resulting in the highest error. Although MAU (Memory Attention Unit) introduces an attention mechanism, its global attention may introduce redundant noise on meteorological grid data characterized by strong local correlations, leading to inferior performance compared to ConvLSTM and CGPR, which are specifically optimized for spatial structure. Figure 5 presents heatmaps of the MAE between the prediction results of different models and the original data. The figure clearly demonstrates the superiority of the CGPR model, outperforming existing models.

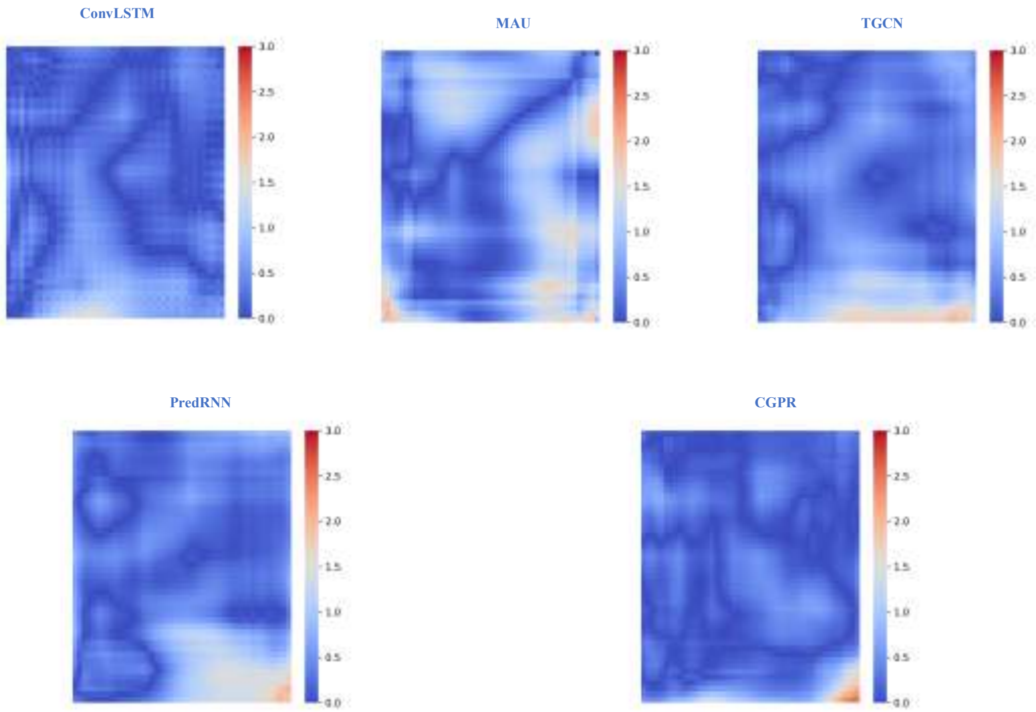

Figure 5: MAE Heatmap of Predictions from Different Models vs. Original Data

4.2. K-value Testing for CGPR

Table 2: Results for Different K-Values

K	MSE	MAE
1	1.614	0.985
3	1.595	0.966
5	**1.561**	**0.897**
7	1.581	0.949

As can be seen from the table, the phenomenon of accuracy gains from increasing the receptive field is observed as K increases from 1 to 5. As K rises from 1 to 5, MSE steadily declines, and MAE shows a significant "jump-like" improvement at K=5 (from 0.966 to 0.897). Here, K represents the order of the Chebyshev polynomial, corresponding to the "neighbor depth" that nodes can aggregate in graph theory. Temperature is influenced not only by local factors but also by surrounding pressure systems and terrain-induced airflows. Therefore, when K=1 or 3, the receptive field is too small, causing the model to act like it is "nearsighted" and unable to capture the effects of long-distance air mass movements. In contrast, K=5 provides sufficient spatial depth, enabling the model to learn the spatiotemporal correlation features across cities within Henan Province (for example, Zhengzhou is jointly influenced by multiple-dimensional nodes such as Anyang, Kaifeng, and Xuchang).

From the table, it is evident that the best performance is achieved at K=5, which corresponds to the peak (lowest point) of the curve. In meteorological grids, K=5 likely covers the core meteorological radius that affects local temperature changes. For a 48×48 grid, a span of 5 steps is sufficient to cover a small- to medium-scale meteorological range, aligning with the characteristics of local weather system evolution in atmospheric science.

As shown in the table, performance declines when K=7. When K increases to 7, the error actually rebounds (MSE rises from 1.561 to 1.581). One possible reason is over-smoothing. In graph neural networks, if the aggregation depth is too high, the features of each node tend to converge to the global average, causing the model to lose its ability to capture "local abrupt temperature changes" (such as sudden cooling from localized heavy rainfall). Another reason could be noise introduction. K=7 incorporates information from overly distant nodes. For Henan's meteorological conditions, weather factors from locations too far away may have weaker correlations with the local area, and forcibly aggregating them may introduce spatial noise. Parameter overfitting is also a possibility. The parameter count of ChebConv increases linearly with K. At K=7, the excessive number of parameters may have led to mild overfitting on the 11,688 days of data.

5. Conclusion

This paper proposes a spatiotemporal temperature prediction model for Henan based on improving PredRNN with ChebConv. By constructing temperature data into a spatiotemporal graph structure, leveraging ChebConv graph convolution to model spatial dependencies, and integrating PredRNN's spatiotemporal memory mechanism to capture temporal dynamics, high-accuracy temperature prediction for Henan is achieved. Experimental results show that by upgrading the underlying operator of PredRNN from spatial convolution to K=5 Chebyshev graph convolution, the spatial heterogeneity issue in temperature prediction for Henan is successfully addressed. The proposed model outperforms all compared models across all evaluation metrics.

Future work can be pursued in the following directions: incorporating multi-source meteorological data (such as humidity, wind speed, etc.) for multivariate prediction; exploring adaptive graph structure learning methods to dynamically adjust spatial dependencies; and extending the model to prediction tasks for other meteorological variables.

References

[1] Menon, S. P., Bharadwaj, R., Shetty, P., Sanu, P. & Nagendra, S. Prediction of temperature using linear regression. in 2017 International Conference on Electrical, Electronics, Communication, Computer, and Optimization Techniques (ICEECCOT) 1–6 (2017). doi:10.1109/ICEECCOT.2017.8284588.

[2] Gupta, I., Mittal, H., Rikhari, D. & Singh, A. K. MLRM: A Multiple Linear Regression based Model for Average Temperature Prediction of A Day. Preprint at https://doi.org/10.48550/arXiv.2203.05835 (2022).

[3] Pang, Z. & Wang, Z. Temperature trend analysis and extreme high temperature prediction based on weighted Markov Model in Lanzhou. Nat Hazards 108, 891–906 (2021).

[4] Johnson, S. D., Battisti, D. S. & Sarachik, E. S. Empirically Derived Markov Models and Prediction of Tropical Pacific Sea Surface Temperature Anomalies. Journal of Climate 13, 3–17 (2000).

[5] Stajkowski, S., Kumar, D., Samui, P., Bonakdari, H. & Gharabaghi, B. Genetic-Algorithm-Optimized Sequential Model for Water Temperature Prediction. Sustainability 12, (2020).

[6] Ren, J., Wang, Z., Pang, Y. & Yuan, Y. Genetic algorithm-assisted an improved AdaBoost double-layer for oil temperature prediction of TBM. Advanced Engineering Informatics 52, 101563 (2022).

[7] Venkadesh, S., Hoogenboom, G., Potter, W. & McClendon, R. A genetic algorithm to refine input data selection for air temperature prediction using artificial neural networks. Applied Soft Computing 13, 2253–2260 (2013).

[8] Quan, Q., Hao, Z., Xifeng, H. & Jingchun, L. Research on water temperature prediction based on improved support vector regression. Neural Comput & Applic 34, 8501–8510 (2022).

[9] Paniagua-Tineo, A. et al. Prediction of daily maximum temperature using a support vector regression algorithm. Renewable Energy 36, 3054–3060 (2011).

[10] Ni, Y. Q., Hua, X. G., Fan, K. Q. & Ko, J. M. Correlating modal properties with temperature using long-term monitoring data and support vector machine technique. Engineering Structures 27, 1762–1773 (2005).

[11] Liu, J. et al. TD-LSTM: Temporal Dependence-Based LSTM Networks for Marine Temperature Prediction. Sensors 18, (2018).

[12] Xiao, C. et al. Short and mid-term sea surface temperature prediction using time-series satellite data and LSTM-AdaBoost combination approach. Remote Sensing of Environment 233, 111358 (2019).

[13] Yang, Y. et al. A CFCC-LSTM Model for Sea Surface Temperature Prediction. IEEE Geoscience and Remote Sensing Letters 15, 207–211 (2018).

[14] Mashaly, A. F. & Alazba, A. A. MLP and MLR models for instantaneous thermal efficiency prediction of solar still under hyper-arid environment. Computers and Electronics in Agriculture 122, 146–155 (2016).

[15] Ghritlahre, H. K. & Prasad, R. K. Exergetic performance prediction of solar air heater using MLP, GRNN and RBF models of artificial neural network technique. Journal of Environmental Management 223, 566–575 (2018).

[16] Chen, Q. et al. TemproNet: A transformer-based deep learning model for seawater temperature prediction. Ocean Engineering 293, 116651 (2024).

[17] Schuster, M. & Paliwal, K. K. Bidirectional recurrent neural networks. IEEE Transactions on Signal Processing 45, 2673–2681 (1997).

[18] Beck, M. et al. xLSTM: Extended Long Short-Term Memory. Preprint at https://doi.org/10.48550/arXiv.2405.04517 (2024).

[19] Shi, X. et al. Convolutional LSTM Network: a machine learning approach for precipitation nowcasting. in Proceedings of the 29th International Conference on Neural Information Processing Systems - Volume 1 vol. 1 802–810 (MIT Press, Cambridge, MA, USA, 2015).

[20] Zhao, L. et al. T-GCN: A Temporal Graph Convolutional Network for Traffic Prediction. IEEE Transactions on Intelligent Transportation Systems 21, 3848–3858 (2020).

[21] Higashiyama, K., Fujimoto, Y. & Hayashi, Y. Feature Extraction of NWP Data for Wind Power Forecasting Using 3D-Convolutional Neural Networks. Energy Procedia 155, 350–358 (2018).

[22] Chang, Z. et al. MAU: A Motion-Aware Unit for Video Prediction and Beyond. in Advances in Neural Information Processing Systems vol. 34 26950–26962 (Curran Associates, Inc., 2021).

[23] Wang, Y. et al. PredRNN: A Recurrent Neural Network for Spatiotemporal Predictive Learning. IEEE Transactions on Pattern Analysis and Machine Intelligence 45, 2208–2225 (2023).